

Article

Dynamic Ferromagnetic Hysteresis Modelling using a Preisach-Recurrent Neural Network Model

Christian Grech ^{1,2,*}, Marco Buzio ², Mariano Pentella ^{2,3} and Nicholas Sammut ^{1,2}

¹ Faculty of Information and Communications Technology, University of Malta, Msida MSD2080, Malta

² CERN, European Organization for Nuclear Research, 1211 Geneva, Switzerland

³ Department of Applied Science and Technology, Politecnico di Torino, 10129 Turin, Italy

* Correspondence: christian.grech.12@um.edu.mt

Version May 10, 2020 submitted to Materials

Abstract: Hysteresis in ferromagnetic materials is a complex physical phenomenon, and its modelling is a challenging problem, especially when dynamic effects are considered. In this work, a Preisach-recurrent neural network model is proposed to predict the dynamic hysteresis in magnetic materials. ARMCO pure iron is used as an important soft magnetic material in particle accelerator magnets. A recurrent neural network coupled with Preisach play operators is proposed, along with a novel validation method for the identification of the model's parameters. The main idea of this work is to create a model which can accurately describe dynamic hysteresis behaviour, given a limited amount of measurements available. The proposed model is found to predict the magnetic flux density of ARMCO pure iron with a Normalised Root Mean Square Error (NRMSE) better than 0.7 %, when trained with just six different hysteresis loops. The model is evaluated using ramp-rates not used in the training procedure, which shows the ability of the model to predict data which has not been measured. The results demonstrate that the Preisach model based on a recurrent neural network can accurately describe ferromagnetic dynamic hysteresis when trained with a limited amount of data, showing the model's potential in the field of materials science.

Keywords: ARMCO pure iron; dynamic hysteresis loop; machine learning; magnetic properties; particle accelerators; Preisach; recurrent neural networks.

1. Introduction

The phenomenon of hysteresis occurs when a system is not only dependent on present input values, but also on past input values. The modelling of hysteresis loops is challenging not only due to the non-linearity exhibited, but in phenomena such as ferromagnetism, dynamic effects add a further aspect of complexity. The interaction between electric and magnetic fields results in induced eddy currents, which cause the magnetic hysteresis characteristics to become wider with respect to the additional losses. Proposed models to predict hysteresis can be classified into two main categories: physical models and phenomenological models. The former type are built on the description of the object being modelled using physics laws. Unfortunately, in most cases such models are mathematically complex and require detailed knowledge of the physical properties of the material being modelled. On the other hand, phenomenological models make use of conventional identification methods, which typically have no physical meaning. Hence, such models are mostly empirical, based on previously acquired experimental data. The most popular phenomenological hysteresis model is the Preisach model [1], used in a vast range of applications. Among the different hysteresis models available in literature, the Preisach-type models prove to have a great potential to explain various magnetization processes, and is one of the most popular models to capture the hysteresis behaviour in

33 non-linear systems.

34

35 The biggest challenge in implementing a Preisach model is the identification of the model
36 parameters, because the use of empirical methods makes the procedure problem-dependent [2].
37 There are numerous identification methods used in literature [3–5]. In most cases, such a function
38 can be identified using measured data and applying a numerical approach, which can be a specific
39 formulation [6,7] or using conventional methods such as an Everett integral [8] or Gaussian/Lorentzian
40 functions [9]. The function can then be applied in software using a look-up table of values. Other
41 ‘black-box’ identification techniques used alongside the Preisach model include genetic algorithms [10],
42 fuzzy models [11] and artificial neural networks (ANN) [12–14]., In [15], Saliah *et al.* showed that
43 using an ANN can match results produced by the conventional methods, considerably reducing the
44 time overhead. In [16], Serpico and Visone build an ANN hysteresis model, which is able to model
45 rate-independent hysteresis when combined with Preisach operators as inputs. Similarly, [17,18] show
46 another two different neural network configurations for modelling the rate-independent hysteresis of
47 magnetic shape memory alloys.

48

49 Another challenge, which arises when using the Preisach model is that the classical model is
50 rate-independent, meaning that the hysteresis output is determined solely by the input’s extreme
51 values, and the input ramp rates do not impact the hysteresis loop. As a result, Mayergoyz [19]
52 introduced the dependence of the weight function on the speed of output variations; similarly, Mrad
53 and Hu [20] and Song and Li [21] proposed an input-rate dependence of the weight function. Both
54 methods suppose the weight function is the right place to add in dynamic behaviors. On the other
55 hand, in [22] a linear dynamic model is added before the classical Preisach operator and the dynamics
56 are assumed to only happen inside the linear dynamic part. The latter cascade structure can be
57 referred to as an ‘external dynamic hysteresis model’ and is found in several works [23–25]. This work
58 will consider the former type of model, where the rate-dependency is considered without including
59 an additional element. This can be accounted for by implementing the Preisach model’s weighting
60 function using dynamic neural networks such as a recurrent neural network (RNN), where each layer
61 has a recurrent connection, allowing the network to have an infinite dynamic response to time series
62 input data. An example of the implementation of such model configurations for hysteretic data can be
63 found in [26], where an Elman RNN was successful in predicting the major loop at several frequencies.
64 In [27], with the addition of Preisach operators at the input stage of an internal time-delay neural
65 network, the major and minor loop hysteresis of a Giant Magnetostrictive Actuator was modelled
66 successfully, however this work did not demonstrate functionality in the saturation regions.

67

68 In this paper, the use of neural networks is proposed to address the challenges presented by
69 classical approaches to identify and estimate dynamic hysteretic systems. A Preisach model is
70 implemented using a single RNN, which is able to predict the different dynamic hysteresis loops
71 of ferromagnetic materials, when a limited amount of measurement data is available. In particular,
72 the model is trained using three particular frequencies and tested on a data set which consists of
73 a different frequency. As a novel contribution to the current research state, both major and minor
74 loop hysteresis are investigated, including saturation regions. The motivation behind this work
75 lies in the prediction of the dynamic behaviour of materials used in the manufacturing of magnets
76 for particle accelerators. As an example, ARMCO is used as part of the superconducting magnets
77 for the High Luminosity upgrade of the Large Hadron Collider at the European Nuclear Research
78 Centre (CERN) [28,29], where pulsed fields are employed. Hence, the knowledge of the material’s
79 dynamic behaviour, which is not easily modelled, is required and this work attempts to propose
80 an accurate model, trained with a limited amount of measurement data, which can also be used at
81 a moderate computational cost. Whilst a vector hysteresis model is required for a 3D model of an
82 accelerator magnet, the model can be used to describe the vertical field used for the RF control of

⁸³ synchrotrons. The description of the eddy-currents transients when ramping up the material during
⁸⁴ a test is complicated due to its hysteretic behaviour and the geometry, generally toroidal, which
⁸⁵ complicates the formulation [30]. This combined with the intrinsic nature of the flux-metric method
⁸⁶ adopted for the material measurement, introduces an uncertainty component on the results, especially
⁸⁷ on the coercive field determination [31,32]. The knowledge of the dynamic behaviour of the material
⁸⁸ can be potentially used to extrapolate the data in DC, allowing the separation of the rate-independent
⁸⁹ hysteresis from the rate-dependent part, and reducing the overall uncertainty.

90

⁹¹ In Section 2, the experimental details behind the measurements, the theory behind the model and
⁹² the validation technique are described. Section 3 describes the results obtained, including the results
⁹³ of a univariate sensitivity analysis. As test material, ARMCO was considered, being an important
⁹⁴ yoke material in particle accelerators [33]. Moreover, having an electrical conductivity in the order
⁹⁵ of 10^8 S/m and a relative permeability in the order of 3000, the effect of the eddy currents on the
⁹⁶ hysteresis loop can be measured with a good signal-to-noise ratio.

⁹⁷ 2. Materials and Methods

⁹⁸ 2.1. Experimental details

⁹⁹ The measurements in this work are performed using a split-coil permeameter [28], shown in
¹⁰⁰ Fig.1, and performed on toroidal test specimens. The equipment consists of three 90-turn coils,
¹⁰¹ separable by means of an opening mechanism. A slot allows the insertion of the sample to be tested in
¹⁰² the permeameter, therefore avoiding the time-demanding operation of a custom coil winding onto
¹⁰³ the sample [34]. The two outermost coils are used as excitation coils and powered in series up to a
¹⁰⁴ maximum current of 40 A, corresponding to a maximum magnetic field of 24 kAm^{-1} . The innermost
¹⁰⁵ coil is used to detect the induced voltage. The entire system is designed to be water cooled, though the
¹⁰⁶ cooling is performed by compressed air.

107



Figure 1. The split-coil permeameter.

The measurements are performed by means of the fluxmetric method, as shown in Fig. 2. The test specimen is magnetized by the two excitation coils, having in total $N_e = 180$ turns and powered in series by a voltage-controlled current generator. Given r_1 and r_2 respectively the inner and the outer radius of the test specimen, the magnetic field is equal to:

$$H(t) = \frac{N_e i(t)}{2\pi r_0} \quad (1)$$

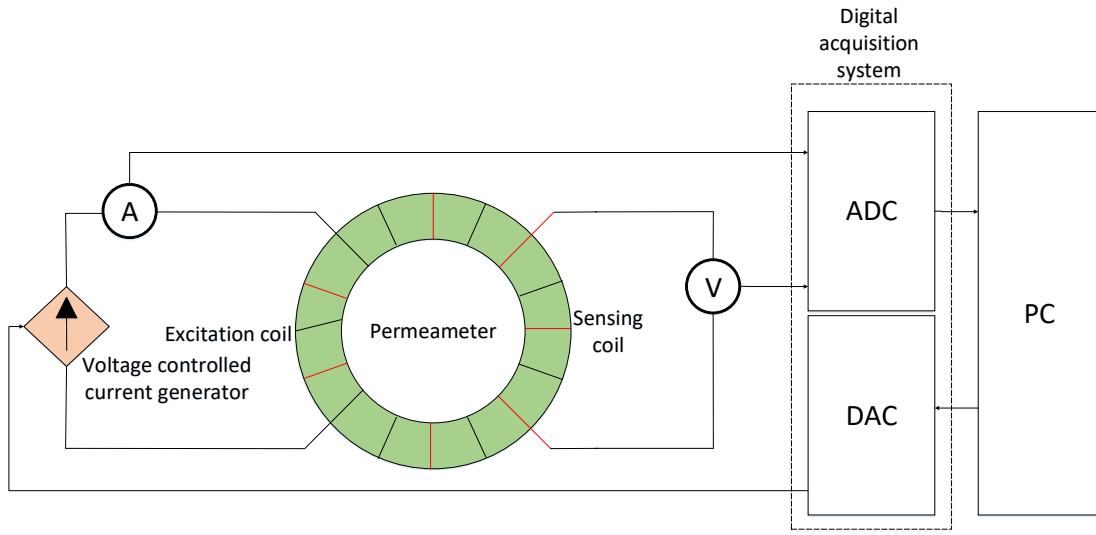


Figure 2. Measurement system layout.

where:

$$r_0 = \frac{r_2 - r_1}{\ln \frac{r_2}{r_1}} \quad (2)$$

Given that the number of turns of the sensing coil, N_s , is equal to 90 turns, the magnetic flux density is evaluated by:

$$B(t) = \frac{1}{A_s} \left(\frac{\Phi(t)}{N_s} - \mu_0 H(A_t - A_s) \right) \quad (3)$$

where A_s is the cross-sectional area of the sample, A_t the cross-sectional area of the sensing coil, μ_0 the permeability of the free space and $\Phi(t)$ the magnetic flux, evaluated by integrating the induced voltage.

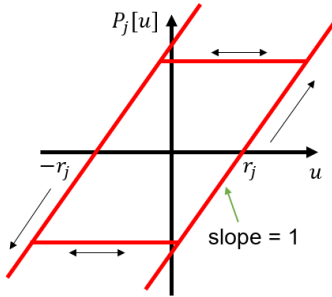
Both the current and the voltage are acquired by a digital acquisition system (DAQ), a NI 4461 [35] by National Instruments at frequency of 20 kHz. In particular, the value of the current is acquired by current transducer, a MACC² PLUS direct current transducer [36]. The value of the magnetic flux density is acquired with an uncertainty of 0.5 mT whereas the magnetic field is known with an accuracy of 0.1 Am^{-1} . The current is ramped back and forth, between positive and negative symmetric values, and at the end of each ramp the current is kept constant for 0.5 s.

For the major hysteresis loops, the plateau amplitudes are chosen in such a way that the material is brought in saturation state. In order to acquire only the hysteresis loop without including the initial magnetization branch, a pre-cycle is applied before the specific cycle. In the case of the minor loops, the same procedure is carried out, with the difference that the plateau amplitudes at each cycle are increased. Between each acquisition and the following one, the sample is demagnetized. The aim of this work is to use these measurements to model the magnetic flux density, $B(t)$ in different dynamic hysteretic conditions using the magnetic field, $H(t)$ as a source of information.

2.2. Hysteresis modelling based on Preisach memory

In general, the Preisach model is expressed using a double integrator in continuous form as [1]:

$$\hat{y}(t) = \int_{\alpha \geq \beta} \int \mu(\alpha, \beta) \gamma_{\alpha\beta} u(t) d\alpha d\beta \quad (4)$$

**Figure 3.** Play operator

where $\hat{y}(t)$ is the model output at time t , $u(t)$ is the model input at time t , while $\gamma_{\alpha\beta}$ are elementary rectangular hysteresis operators with α and β being the up and down switching values, respectively. These operators can only assume a value of $+1$ or -1 . The density function $\mu(\alpha, \beta)$ is a weighting function, which represents the only model unknown which has to be determined from experimental data. In [37,38], following a change in co-ordinates $r = (\alpha - \beta)/2$, $v = (\alpha + \beta)$, $\hat{\mu} = \mu(v + r, v - r)$, it is shown that the boundary between the $+1$ and -1 regions in the Preisach half-plane with coordinates $r > 0$, $v \in \mathbb{R}$, is described by the function $v = P[u](t)$, known as the play operator. This makes it possible to rearrange Eq. 4 as:

$$\hat{y}(t) = \int_0^{+\infty} g(r, P[u(t)]) dr \quad (5)$$

which can be discretized to n play operators as follows:

$$\hat{y}(t) = \sum_{j=1}^n \phi_j P_j[u](t) \quad (6)$$

where ϕ_j represents the density function of the j th play operator, which has to be identified. The play operator is shown in Fig. 3, and defined in Eq. 7:

$$P_j[u](t) = \max(u(t) - r_j, \min(u(t) + r_j, P_j[u](t - 1))) \quad (7)$$

$$P_j[0] = \max(u(0) - r_j, \min(u(0) + r_j, k_0)) \quad (8)$$

where k_0 is the initial condition of the operator and r_j represents the memory depth as follows:

$$r_j = \frac{j-1}{n} [\max(u(t)) - \min(u(t))] \quad (9)$$

¹²⁹ where $j = 1, 2, 3, \dots, n$.

¹³⁰

¹³¹ *2.3. Identifying ϕ using recurrent neural networks*

¹³² Artificial neural networks are able to map non-linear data in various applications. In this case, a
¹³³ recurrent neural network (RNN) will be used to replace the density function ϕ_j of the discrete Preisach
¹³⁴ model (Eq. 6), as these structures are recognized for their ability to model any non-linear dynamic
¹³⁵ system, up to a given degree of accuracy [39]. RNNs are distinguished from feed-forward networks by
¹³⁶ the feedback loop connected to their past decisions, ingesting their own outputs moment after moment
¹³⁷ as input. This means that such networks can be used to model dynamic characteristics. Sequential
¹³⁸ information is preserved in the recurrent network's context layer, which manages to span many time
¹³⁹ steps as it cascades forward to affect the processing of each new example.

¹⁴⁰

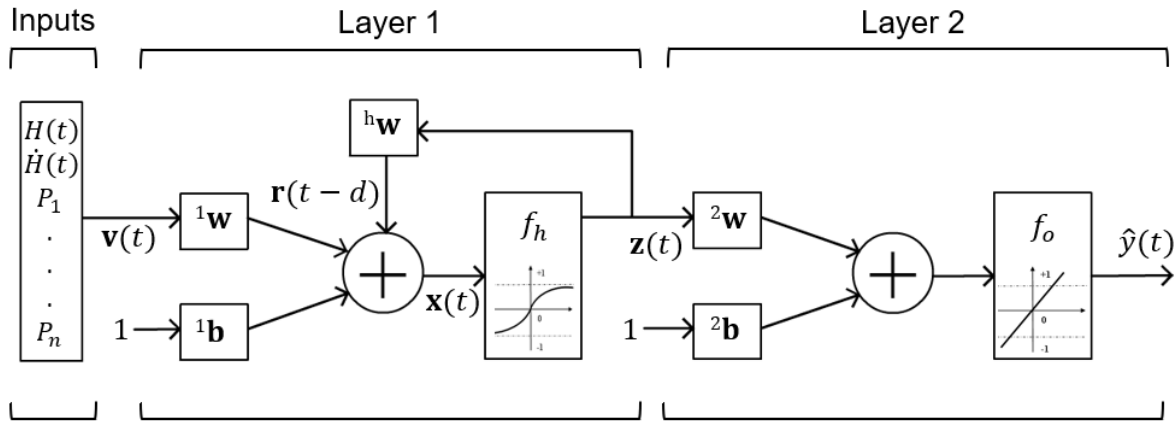


Figure 4. Schematic diagram of the Preisach-RNN model.

In general, a RNN can be seen as a group of nodes, consisting of three different kinds of nodes, namely the input, hidden and output nodes, organized in three separate layers, as shown in Fig. 4. While the input and output layers consist of feed-forward connections, the hidden layer has recurrent ones. At each time step, t , the input vector $\mathbf{v}(t)$ is processed at the input layer. Each instant $\mathbf{v}(t)$ is summed with the bias vector $^1\mathbf{b}$ and multiplied by the input weight matrix $^1\mathbf{w}$. Analogously, the internal state $\mathbf{z}(t)$, delayed by a number of time instants d , is multiplied by the gain factor $^h\mathbf{w}$ and added to the input state as follows:

$$\mathbf{z}(t) = f_h[^1\mathbf{w}(\mathbf{v}(t) + ^1\mathbf{b}) + ^h\mathbf{w}(\mathbf{z}(t-d))] \quad (10)$$

where $f_h(x)$ is the activation function, in this case a hyperbolic tangent function, which is given as:

$$f_h(x) = \frac{2}{1 + e^{-2x}} - 1 \quad (11)$$

The internal state $\mathbf{z}(t)$ is then added with bias $^2\mathbf{b}$, multiplied by the weight $^2\mathbf{w}$, and the result is passed through a linear activation function $f_o(x)$ as follows:

$$\hat{y}(t) = f_o[^2\mathbf{w}(\mathbf{z}(t) + ^2\mathbf{b})] \quad (12)$$

where $\hat{y}(t)$ is the predicted output at time t .

The Deep Learning Toolbox [40] by MATLAB is used to determine the weights of the network using the *layrecnet* command. The training algorithm is the Levenberg-Marquadt algorithm [41], which is a non-linear least squares optimization algorithm incorporated into the backpropagation algorithm for training neural networks as demonstrated in detail in [42]. The algorithm aims to optimize the weights according to the following objective function:

$$V(t) = \frac{1}{2}(\mathbf{y}(t) - \hat{\mathbf{y}}(t))^T(\mathbf{y}(t) - \hat{\mathbf{y}}(t)) \quad (13)$$

which leads to the update of the weights by the following formula:

$$^i\mathbf{w}(t+1) = ^i\mathbf{w}(t) + \eta \left(-\frac{\partial V}{\partial t} \right) \quad (14)$$

where η is a positive number representing the learning rate of the weights.

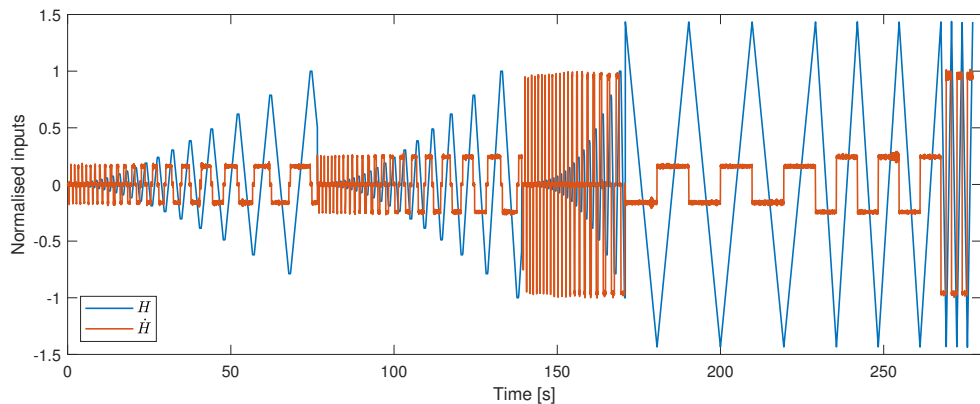


Figure 5. Magnetic field data and its derivative used for training, validation and testing the model.

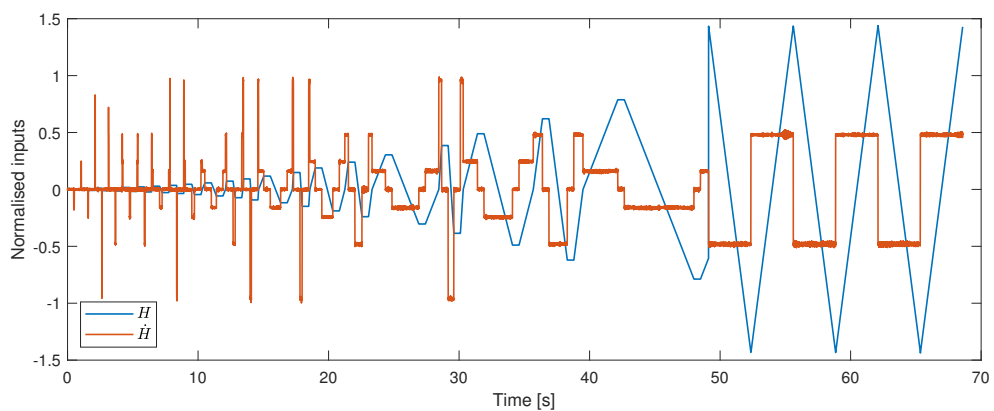


Figure 6. Magnetic field data and its derivative used for evaluating the model.

151 2.4. Data analysis approach

152 The input data to the model include the magnetic field $H(t)$, its derivative $\dot{H}(t)$ and a number of
 153 play operators $P_j[H](t)$ (chosen according to the complexity of the data). All data is normalised to the
 154 range of the minor loop data, such that data is approximately in the range $[-1, 1]$. The play operator
 155 outputs, P_j , are subsequently calculated based on the normalised magnetic field signal. In this work,
 156 the predicted variable is the magnetic flux density measured in Section 2.1, and all measurements are
 157 downsampled to 200 Hz.

158

159 The data set used for training, validation and testing comprises of three minor loops and three
 160 major loops ramping at $1025, 1554$ and $6135 \text{ Am}^{-1}\text{s}^{-1}$, as shown in Fig. 5. This data is divided into
 161 three subsets in an interleaved manner. The first subset is the training set (70% of the data), which
 162 is used for updating the network weights and biases. The second subset is the validation set (15%
 163 of the data), used to decide when to stop training the model, whilst the final set is the testing set
 164 (15% of the data), which is used to select the best model structure. Once the network is trained, and
 165 the best model structure is chosen, an evaluation signal is used to demonstrate the performance of
 166 the model. The evaluation data set consists of three major loops ramping at $3067 \text{ Am}^{-1}\text{s}^{-1}$ and one
 167 minor loop ramping at various random ramp-rates between 1000 and $6200 \text{ Am}^{-1}\text{s}^{-1}$, as shown in Fig. 6.
 168

169 2.5. Model validation

170 Model validation is the process of choosing the best model parameters and making sure that the
 171 model is robust to new data. The optimal number of nodes in the hidden layer, h is chosen by doing a

¹⁷² search over a range of values. The complete validation process explained below consists of three loops,
¹⁷³ and is represented by a flowchart in Fig. 7.

¹⁷⁴

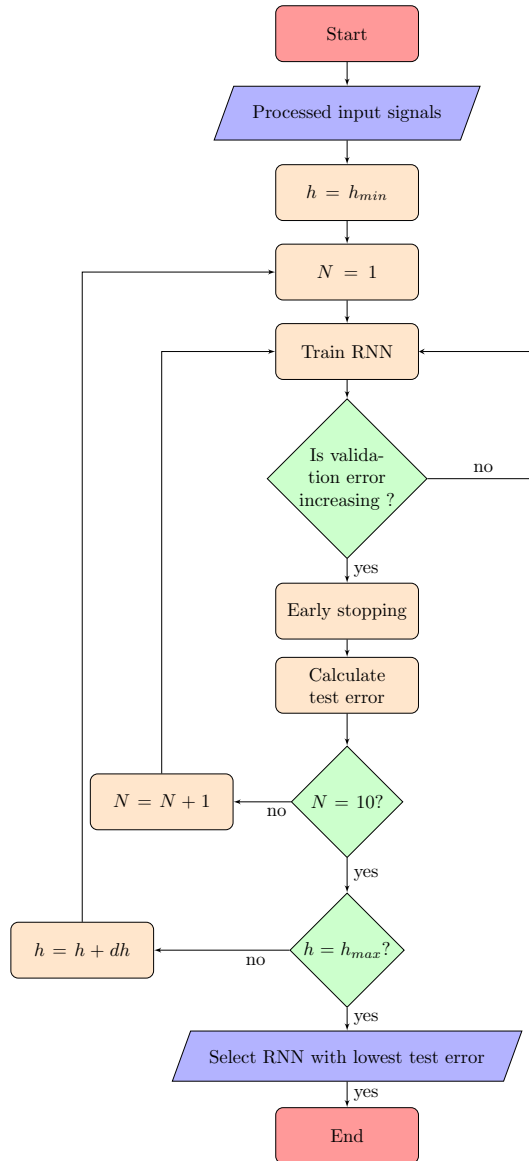


Figure 7. Flowchart showing the model training and validation procedure

¹⁷⁵ In the innermost loop, each neural network is trained using the training set as described in
¹⁷⁶ Section 2.3 over a certain number of repetitions called epochs. The number of epochs is determined
¹⁷⁷ using a method called early stopping [43,44]. In this technique, the error on the validation set is
¹⁷⁸ monitored during the training process. The validation error normally decreases during the initial
¹⁷⁹ phase of training, as does the training set error. However, when the network begins to overfit the
¹⁸⁰ data, the error on the validation set typically begins to rise. When the validation error increases for a
¹⁸¹ specified number of iterations, the training is stopped, and the weights and biases at the minimum
¹⁸² of the validation error are returned. Finally, the testing set is used to obtain the performance of the
¹⁸³ particular network.

¹⁸⁴

¹⁸⁵ Each time a neural network is trained, a different solution is obtained due to different and random
¹⁸⁶ initial weight and bias values. As a result, different neural networks trained on the same problem can

¹⁸⁷ give different outputs for the same input. To ensure that a neural network of good accuracy has been
¹⁸⁸ found, each network is retrained for a number of times, N , which in this work is 10.

¹⁸⁹

¹⁹⁰ In the outermost loop, the number of hidden nodes is varied over the range starting from h_{min} to
¹⁹¹ h_{max} with increments of dh . The network with the best test performance having a number of hidden
¹⁹² nodes h , is hence chosen and used with the evaluation data set. The complete list of parameters used
¹⁹³ in this work is given in Table 1.

¹⁹⁴

Table 1. RNN parameters list

	Parameter	Value
Model properties	Activation function (hidden layer)	sigmoid
	Activation function (output layer)	linear
	delay, d	2
	hidden nodes search range, $h_{min} : dh : h_{max}$	4:1:13
	number of hidden nodes, h	12
	training repetitions, N	10
Input	No. of play operators	6
Training set	data	70% of data set
	epochs	≤ 1000
	algorithm	Levenberg-Marquadt
Validation set	data	15% of data set
Testing set	data	15% of data set
Evaluation set	data	unseen data
	metric	NRMSE

¹⁹⁵ 2.6. Performance indicator

The performance indicator used in this work to represent the error between the model and experimental measurements is the normalised root mean square error (NRMSE):

$$\text{NRMSE}(y, \hat{y}) = \frac{1}{\max(y) - \min(y)} \sqrt{\frac{1}{N} \sum_{i=1}^N (y_i - \hat{y}_i)^2} \quad (15)$$

¹⁹⁶ where y is the actual value, \hat{y} is the modelled quantity and N is the number of samples considered.
¹⁹⁷ By normalising the root mean square error, the errors can be scaled relatively to the range of the
¹⁹⁸ measurement, thus allowing an appropriate comparison across different conditions.

¹⁹⁹ 3. Results

²⁰⁰ Results from the model training, testing and sensitivity analysis are presented and discussed in
²⁰¹ this section.

²⁰² 3.1. Minor and major loop model prediction

²⁰³ Following the model validation and training procedure explained in the previous section, the best
²⁰⁴ performing model is used for predicting the data in the evaluation set shown in Fig. 6. In order to get
²⁰⁵ rid of the initial transient phase of the model, the first few predicted samples in the set are discarded.
²⁰⁶ In the case of the major loop, a NRMSE of 0.58 % is noted in predicting a hysteresis loop with a new
²⁰⁷ ramp-rate not used for training. Fig. 8 shows the major loop data used for training and evaluating

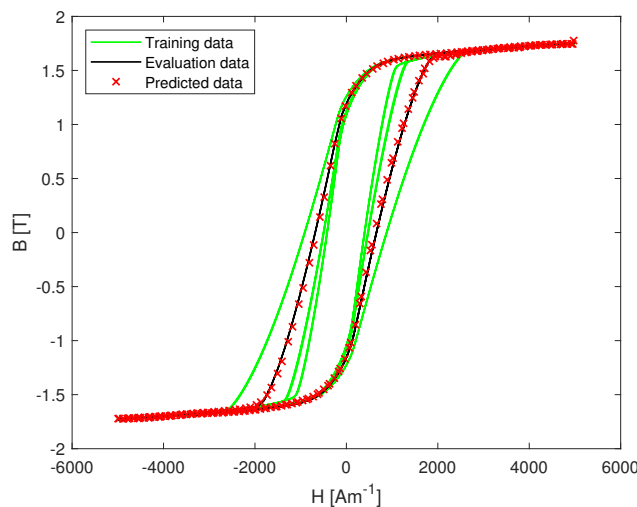


Figure 8. Predicted major loop and experimental data used in training the model

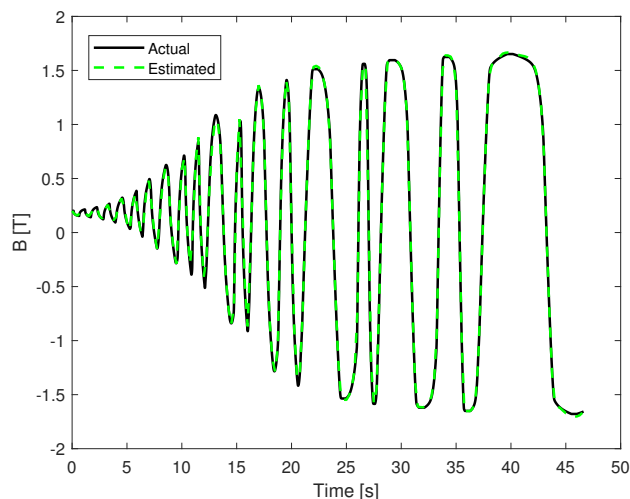


Figure 9. Predicted minor loop with random ramp-rates

the model, as well as the predicted data. For the minor loop data, a NRMSE of 0.66 % is noted with different random ramp-rates, including ramp-rates not used for training the model. The magnetic flux density as a function of time is shown in Fig. 9.

3.2. Effect of Preisach operators on performance

In order to quantify the impact of Preisach operators as part of the model, the model's training and validation procedure is repeated without the P_j inputs. Comparing the performance of the two models, the inclusion of the Preisach operators is noted to improve performance by 19 % in the case of major loop hysteresis, and 44 % in the case of minor loop hysteresis. It has to be noted however, that a model without Preisach operators is computationally less expensive, as the optimal structure contains 241 weights versus 409 weights in the original model. Hence, in the end, a compromise must be made between accuracy and speed according to the model's application.

3.3. Univariate sensitivity analysis

A univariate sensitivity analysis provides information on how robust a model is when the input values are varied over a specific range [45]. This analysis is performed to understand which model

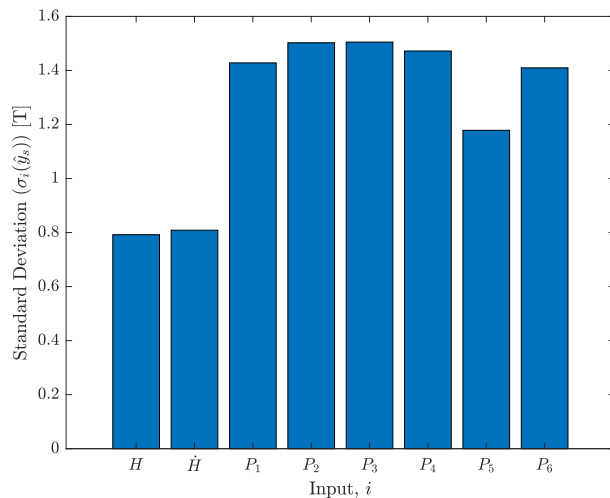


Figure 10. Sensitivity analysis results for each individual input.

222 input variables impact the prediction most significantly, especially since the magnetic field derivative
 223 signal, $\dot{H}(t) +$ is noisy. A neural network which picks up minor noise during training can overfit the
 224 noise as if it is the signal, leading to poor accuracy during validation [46]. One way to confirm this
 225 is by performing a sensitivity analysis, where one input parameter is fed a changing signal whilst
 226 keeping the other inputs constant, and checking the deviation in the output signal. This is repeated for
 227 all the model inputs.

228

229 In this exercise, once the model is trained, an input vector is defined and set as 0. Then, for
 230 one of the eight variables, a value is assigned between the [-1,1] range. This is repeated for 10,000
 231 samples for each input variable. The predicted output, \hat{y}_s is saved and the standard deviation $\sigma_i(\hat{y}_s)$
 232 for each variable i is calculated. The bar chart in Fig. 10 illustrates these results. The analysis results
 233 show a higher variation in the predicted output for play operator input parameters, thus the model is
 234 more sensitive to changes in these particular variables. These results also confirm the fact that even
 235 though the model is trained with a noisy \dot{H} signal, the predicted output is not particularly sensitive to
 236 perturbations from this parameter.

237 4. Conclusions

238 A Preisach-RNN model is proposed to predict the dynamic characteristics of ferromagnetic
 239 materials that does not require *a priori* knowledge of the material and its microstructural behaviour.
 240 The model is based on the Preisach memory block where the density function is represented by a
 241 recurrent neural network. A thorough training and validation procedure is proposed for the neural
 242 network, in order to optimize the weight parameters. We have demonstrated, using ARMCO pure
 243 iron measurements, that such a model can predict both major and minor loop dynamic ferromagnetic
 244 hysteresis behaviour allowing researchers to estimate the dynamic effects of the material knowing
 245 only six different examples at three frequencies. Comparing the model's predictions to experimental
 246 data, the model's NRMSE is noted to be better than 0.7 %. Moreover, these results prove that the
 247 model generalises well to new data. In validating the performance of the model, the positive impact of
 248 Preisach operators is noted, even though this comes at a computational cost. Results from a univariate
 249 sensitivity analysis also demonstrate that the play operator inputs impact the predicted magnetic flux
 250 output most significantly. We believe that this model, predicting major and minor loop hysteresis
 251 under different dynamic conditions can be applied to other dynamic hysteresis prediction problems in
 252 the realm of materials science.

Author Contributions: Conceptualization, C.G., M.B., M.P. and N.S.; methodology, C.G. and M.P.; software, C.G., and M.P.; validation, C.G.; formal analysis, C.G. and M.P.; investigation, C.G. and M.P.; data curation, C.G. and M.P.; writing—original draft preparation, C.G. and M.P.; writing—review and editing, C.G., M.B., M.P. and N.S.; visualization, C.G.; supervision, M.B. and N.S.

Funding: This research received no external funding. The publication fee was funded by CERN.

Conflicts of Interest: The authors declare no conflict of interest.

Abbreviations

The following abbreviations are used in this manuscript:

ANN	Artificial Neural Network
CERN	European Organization for Nuclear Research
NRMSE	Normalised Root Mean Square Error
RNN	Recurrent Neural Network

1. Mayergoyz, I. Chapter 1 - The Classical Preisach Model of Hysteresis. In *Mathematical Models of Hysteresis and Their Applications*; Mayergoyz, I., Ed.; Electromagnetism, Elsevier Science: New York, 2003; pp. 1 – 63. doi:<https://doi.org/10.1016/B978-012480873-7/50002-5>.
2. Saliah, H.; Lowther, D. The use of neural networks in magnetic hysteresis identification. *Physica B: Condensed Matter* **1997**, *233*, 318 – 323. Hysteresis Modeling and Micromagnetism, doi:[https://doi.org/10.1016/S0921-4526\(97\)00316-5](https://doi.org/10.1016/S0921-4526(97)00316-5).
3. Iyer, R.V.; Tan, X. Control of hysteretic systems through inverse compensation. *IEEE Control Systems Magazine* **2009**, *29*, 83–99. doi:[10.1109/MCS.2008.930924](https://doi.org/10.1109/MCS.2008.930924).
4. Sutor, A.; Rupitsch, S.J.; Lerch, R. A Preisach-based hysteresis model for magnetic and ferroelectric hysteresis. *Applied Physics A* **2010**, *100*, 425–430. doi:[10.1007/s00339-010-5884-9](https://doi.org/10.1007/s00339-010-5884-9).
5. Stakvik, J. Identification, Inversion and Implementaion of the Preisach Hysteresis Model in Nanopositioning. Master's thesis, Nowegian University of Science and Technology, 2014.
6. Biorci, G.; Pescetti, D. Analytical theory of the behaviour of ferromagnetic materials. *Il Nuovo Cimento (1955-1965)* **1958**, *7*, 829–842. doi:[10.1007/BF02745588](https://doi.org/10.1007/BF02745588).
7. Ruderman, M.; Bertram, T. Identification of Soft Magnetic B-H Characteristics Using Discrete Dynamic Preisach Model and Single Measured Hysteresis Loop. *IEEE Transactions on Magnetics* **2012**, *48*, 1281–1284. doi:[10.1109/TMAG.2011.2172931](https://doi.org/10.1109/TMAG.2011.2172931).
8. Kozek, M.; Gross, B. Identification and Inversion of Magnetic Hysteresis for Sinusoidal Magnetization. *International Journal of Online and Biomedical Engineering* **2005**.
9. Rouve, L.; Waeckerle, T.; Kedous-Lebouc, A. Application of Preisach model to grain oriented steels: comparison of different characterizations for the Preisach function $p(\alpha, \beta)$. *IEEE Transactions on Magnetics* **1995**, *31*, 3557–3559. doi:[10.1109/20.489568](https://doi.org/10.1109/20.489568).
10. Hergli, K.; Marouani, H.; Zidi, M.; Fouad, Y.; Elshazly, M. Identification of Preisach hysteresis model parameters using genetic algorithms. *Journal of King Saud University - Science* **2017**. doi:[10.1016/j.jksus.2017.11.005](https://doi.org/10.1016/j.jksus.2017.11.005).
11. Natale, C.; Velardi, F.; Visone, C. Identification and compensation of Preisach hysteresis models for magnetostrictive actuators. *Physica B: Condensed Matter* **2001**, *306*, 161 – 165. Proceedings of the Third International Symposium on Hysteresis an d Micromagnetics Modeling, doi:[https://doi.org/10.1016/S0921-4526\(01\)00997-8](https://doi.org/10.1016/S0921-4526(01)00997-8).
12. Adly, A.; El-Hafiz, S.A. Using neural networks in the identification of Preisach-type hysteresis models. *IEEE Transactions on Magnetics* **1998**, *34*, 629–635. doi:[10.1109/20.668057](https://doi.org/10.1109/20.668057).
13. Akbarzadeh, V.; Davoudpour, M.; Sadeghian, A. Neural network modeling of magnetic hysteresis. *2008 IEEE International Conference on Emerging Technologies and Factory Automation* **2008**, pp. 1267–1270.
14. Firouzi, M.; Shouraki, S.B.; Zakerzadeh, M.R. Hysteresis nonlinearity identification by using RBF neural network approach. *2010 18th Iranian Conference on Electrical Engineering*. IEEE, 2010. doi:[10.1109/iranianee.2010.5506985](https://doi.org/10.1109/iranianee.2010.5506985).

- 300 15. Saliah, H.H.; Lowther, D.A.; Forghani, B. A neural network model of magnetic hysteresis for computational
301 magnetics. *IEEE Transactions on Magnetics* **1997**, *33*, 4146–4148. doi:10.1109/20.619691.
- 302 16. Serpico, C.; Visone, C. Magnetic hysteresis modeling via feed-forward neural networks. *IEEE Transactions
303 on Magnetics* **1998**, *34*, 623–628. doi:10.1109/20.668055.
- 304 17. Xu, R.; Zhou, M. Elman Neural Network-Based Identification of Krasnosel'skii-Pokrovskii Model
305 for Magnetic Shape Memory Alloys Actuator. *IEEE Transactions on Magnetics* **2017**, *53*, 1–4.
306 doi:10.1109/TMAG.2017.2700479.
- 307 18. Zhou, M.; Zhang, Q. Hysteresis Model of Magnetically Controlled Shape Memory Alloy Based on a PID
308 Neural Network. *IEEE Transactions on Magnetics* **2015**, *51*, 1–4. doi:10.1109/tmag.2015.2434933.
- 309 19. Mayergoyz, I.D. Dynamic Preisach models of hysteresis. *IEEE Transactions on Magnetics* **1988**, *24*, 2925–2927.
310 doi:10.1109/20.92290.
- 311 20. Mrad, R.B.; Hu, H. Dynamic modeling of hysteresis in piezoceramics. 2001 IEEE/ASME International
312 Conference on Advanced Intelligent Mechatronics. Proceedings (Cat. No.01TH8556). IEEE, 2001.
313 doi:10.1109/aim.2001.936515.
- 314 21. Song, D.; Li, C.J. Modeling of piezo actuator's nonlinear and frequency dependent dynamics. *Mechatronics*
315 **1999**, *9*, 391 – 410. doi:[https://doi.org/10.1016/S0957-4158\(99\)00005-7](https://doi.org/10.1016/S0957-4158(99)00005-7).
- 316 22. Füzi, J. Computationally efficient rate dependent hysteresis model. *COMPEL - The International
317 Journal for Computation and Mathematics in Electrical and Electronic Engineering* **1999**, *18*, 445–457.
318 doi:10.1108/03321649910275080.
- 319 23. Kuczmann, M. Dynamic Preisach model identification applying FEM and measured BH curve. *COMPEL - The
320 International Journal for Computation and Mathematics in Electrical and Electronic Engineering* **2014**,
321 *33*, 2043–2052. doi:10.1108/COMPEL-11-2013-0368.
- 322 24. Makaveev, D.; Dupré, L.; Wulf, M.D.; Melkebeek, J. Dynamic hysteresis modelling using
323 feed-forward neural networks. *Journal of Magnetism and Magnetic Materials* **2003**, *254*-255, 256
324 – 258. Proceedings of the 15th International Conference on Soft Magnetic Materials (SMM15),
325 doi:[https://doi.org/10.1016/S0304-8853\(02\)00785-0](https://doi.org/10.1016/S0304-8853(02)00785-0).
- 326 25. Tan, X.; Baras, J.S. Modeling and control of hysteresis in magnetostrictive actuators. *Automatica* **2004**,
327 *40*, 1469–1480. doi:10.1016/j.automatica.2004.04.006.
- 328 26. Saghafifar, M.; Kundu, A.; Nafalski, A. Dynamic magnetic hysteresis modelling using Elman recurrent
329 neural network. *International Journal of Applied Electromagnetics and Mechanics* **2001**, *13*, 209–214.
- 330 27. Wang, Q.; Su, C.Y.; Tan, Y. On the Control of Plants with Hysteresis : Overview and a Prandtl-Ishlinskii
331 Hysteresis Based Control Approach. *ACTA Automatica Sinica*, 2005.
- 332 28. Parrella, A.; Arpaia, P.; Buzio, M.; Liccardo, A.; Pentella, M.; Principe, R.; Ramos, P. Magnetic Properties of
333 Pure Iron for the Upgrade of the LHC Superconducting Dipole and Quadrupole Magnets. *IEEE Transactions
334 on Magnetics* **2018**, *55*, 1–4.
- 335 29. Arpaia, P.; Buzio, M.; Bermudez, S.I.; Liccardo, A.; Parrella, A.; Pentella, M.; Ramos, P.M.; Stubberud,
336 E. A Superconducting Permeameter for Characterizing Soft Magnetic Materials at High Fields. *IEEE
337 Transactions on Instrumentation and Measurement* **2019**.
- 338 30. Namjoshi, K.; Lavers, J.D.; Biringer, P. Eddy-current power loss in toroidal cores with rectangular cross
339 section. *IEEE transactions on magnetics* **1998**, *34*, 636–641.
- 340 31. Anglada, J.; Arpaia, P.; Buzio, M.; Pentella, M.; Petrone, C. Characterization of Magnetic Steels for the
341 FCC-ee Magnet Prototypes **2018**. *55*, 1–4.
- 342 32. Grossinger, R.; Mehboob, N.; Suess, D.; Turtelli, R.S.; Kriegisch, M. An eddy-current model describing the
343 frequency dependence of the coercivity of polycrystalline Galfenol. *IEEE Transactions on Magnetics* **2012**,
344 *48*, 3076–3079.
- 345 33. Sgobba, S. Physics and measurements of magnetic materials **2011**. p. 25 p. presented at the CERN Accelerator School CAS 2009: Specialised Course on Magnets, Bruges, 16-25 June 2009,
346 doi:10.5170/CERN-2010-004.39.
- 348 34. Arpaia, P.; Buzio, M.; Fiscarelli, L.; Montenero, G.; Walckiers, L. High-performance permeability
349 measurements: A case study at CERN. 2010 IEEE Instrumentation & Measurement Technology Conference
350 Proceedings. IEEE, 2010, pp. 58–61.
- 351 35. National Instruments. *NI 446x Specifications*, 2008. Available: <http://www.ni.com/pdf/manuals/373770j.pdf>.

- 353 36. Hitec. *MACC 2 plus*, 2016. Available: <http://www.pm-sms.com/files/2016/02/Specifications-MACC-2-plus.pdf>.
- 354 37. Krejčí, P. On Maxwell equations with the Preisach hysteresis operator: The one-dimensional time-periodic
355 case. *Aplikace matematiky* **1989**, *34*, 364–374.
- 356 38. Brokate, M. Some mathematical properties of the Preisach model for hysteresis. *IEEE Transactions on
358 Magnetics* **1989**, *25*, 2922–2924. doi:10.1109/20.34325.
- 359 39. Schäfer, A.M.; Zimmermann, H.G. Recurrent Neural Networks are universal approximators. *International
360 Journal of Neural Systems* **2007**, *17*, 253–263, [<https://doi.org/10.1142/S0129065707001111>]. PMID: 17696290,
361 doi:10.1142/S0129065707001111.
- 362 40. MATLAB. *Deep Learning Toolbox*, 2019. Available: https://www.mathworks.com/help/deeplearning/index.html?s_tid=mwa_osa_a.
- 363 41. Marquardt, D. An Algorithm for Least-Squares Estimation of Nonlinear Parameters. *Journal of
365 the Society for Industrial and Applied Mathematics* **1963**, *11*, 431–441, [<https://doi.org/10.1137/0111030>].
366 doi:10.1137/0111030.
- 367 42. Hagan, M.T.; Menhaj, M.B. Training feedforward networks with the Marquardt algorithm. *IEEE
368 Transactions on Neural Networks* **1994**, *5*, 989–993.
- 369 43. Prechelt, L., Early Stopping — But When? In *Neural Networks: Tricks of the Trade: Second Edition*; Springer
370 Berlin Heidelberg: Berlin, Heidelberg, 2012; pp. 53–67. doi:10.1007/978-3-642-35289-8_5.
- 371 44. Yao, Y.; Rosasco, L.; Caponnetto, A. On Early Stopping in Gradient Descent Learning. *Constructive
372 Approximation* **2007**, *26*, 289–315. doi:10.1007/s00365-006-0663-2.
- 373 45. Salciccioli, J.D.; Crutain, Y.; Komorowski, M.; Marshall, D.C., Sensitivity Analysis and Model Validation. In
374 *Secondary Analysis of Electronic Health Records*; Springer International Publishing: Cham, 2016; pp. 263–271.
375 doi:10.1007/978-3-319-43742-2_17.
- 376 46. Liu, Z.P.; Castagna, J.P. Avoiding overfitting caused by noise using a uniform training mode. IJCNN'99.
377 International Joint Conference on Neural Networks. Proceedings (Cat. No.99CH36339), 1999, Vol. 3, pp.
378 1788–1793 vol.3. doi:10.1109/IJCNN.1999.832649.

379 © 2020 by the authors. Submitted to *Materials* for possible open access publication under the terms and conditions
380 of the Creative Commons Attribution (CC BY) license (<http://creativecommons.org/licenses/by/4.0/>).